Reduced model and application of inflating circular diaphragm dielectric elastomer generators for wave energy harvesting

(Article begins on next page)

30 January 2025

REDUCED MODEL AND APPLICATION OF INFLATING CIRCULAR DIAPHRAGM DIELECTRIC ELASTOMER GENERATORS FOR WAVE ENERGY HARVESTING

Rocco Vertechy*

PERCRO SEES, TeCIP Institute, Scuola Superiore Sant'Anna

Piazza Martiri della Libertà 33, 5612, Pisa, Italy

e-mail: r.vertechy@sssup.it

Gastone Pietro Papini Rosati

PERCRO SEES, TeCIP Institute, Scuola Superiore Sant'Anna

Piazza Martiri della Libertà 33, 5612, Pisa, Italy

e-mail: g.rosatipapini@sssup.it

Marco Fontana

PERCRO SEES, TeCIP Institute, Scuola Superiore Sant'Anna

Piazza Martiri della Libertà 33, 5612, Pisa, Italy

e-mail: m.fontana@sssup.it

*Corresponding author

ABSTRACT

Dielectric elastomers are incompressible rubber-like solids whose electrical and structural responses are highly non-linear and strongly coupled. Thanks to their coupled electro-mechanical response, intrinsic lightness, easy-manufacturability and low-cost, DEs are perfectly suited for the development of novel solid-state polymeric energy conversion units with capacitive nature and high-voltage operation, which are more resilient, lightweight, integrated, economic and disposable than traditional generators based on conventional electromagnetic technology. Inflated Circular Diaphragm Dielectric Elastomer Generators (ICD-DEGs) are a special embodiment of polymeric transducer that can be used to convert pneumatic energy into usable electricity. Potential application of ICD-DEGs is as power take-off system for wave energy converters based on the Oscillating Water Column (OWC) principle. This paper presents a reduced, yet accurate, dynamic model for ICD-DEGs that features one kinematic degree of freedom and which accounts for dielectric elastomer visco-elasticity. The model is computationally simple and can be easily integrated into existing wave-to-wire models of OWCs to be used for fast analysis and real-time applications. For demonstration purposes, integration of the considered ICD-DEG model with a lumped-parameter hydrodynamic model of a realistic OWC is also presented along with a simulation case study.

INTRODUCTION

Dielectric elastomer transducers are a promising technology for the development of solid-state actuators, sensors and generators [1]. Dielectric elastomer transducers comprise one or more sheets of

incompressible dielectric rubber that are sandwiched between compliant electrodes to form a deformable capacitor. In actuator mode, electrostatic attraction between oppositely charged electrodes is used to convert electricity into mechanical energy. In sensor mode, measurements of the electrical impedance of the deformable transducer are used to infer strains or stresses (that is, displacements or forces). In generator mode, mechanical energy is converted into direct electricity via the variable-capacitance electrostatic generator principle.

Properties of DEs which make them suited for transduction applications are: low mass density; large deformability; high energy density; rather good electro-mechanical conversion efficiency; moderate or low cost; solid-state monolithic embodiment with no sliding parts; easy to manufacture, assemble and recycle; good chemical resistance to corrosive environments; silent operation.

Initially proposed as muscle-like actuators for robots, DEs are now receiving significant attention for energy scavenging applications [2-6]. Their intrinsically cyclical operation makes them particularly suited for the development of Wave Energy Converters (WECs) [7-12]. Specifically, Dielectric Elastomer Generators (DEGs) are foreseen to replace the power take-off systems of traditional WECs, which are currently made of stiff, heavy, shock-sensitive, corrosion-sensitive and costly (metallic and rare-earth) materials. Expected advantages of DEG power take-off systems are: ease of installation and maintenance, low capital and operating costs, shock and corrosion insensitivity, noise and vibration free operation, high energy conversion efficiency that is independent of sea-wave period.

A very interesting concept of a DEG-based WEC is the Polymeric Oscillating Water Column (Poly-OWC) [9] that is shown in Figure 1. A Poly-OWC is a partially submerged hollow structure featuring an immersed part opened to the sea action, and an upper part closed by a DEG membrane

forming an air chamber. The structure partially encloses a column of water that is exposed to the incident wave field at the bottom and to the chamber air pressure at the top. As the waves impinge on the Poly-OWC structure, wave-induced pressure oscillations at the underwater interface cause the reciprocating motion of the water column, with a concomitant compression-expansion of the air entrapped in the upper chamber, and the resulting inflation-deflation of the DEG membrane. To generate electricity, electric charges are put on the DEG electrodes when the membrane is expanded in area. As the membrane contracts, DEG capacitance decreases, which makes the charges increase their electric potential, thereby converting the work done by the air-chamber pressure on the DEG membrane into usable direct current electricity.

In previous works, the potentialities of Poly-OWCs have been investigated: 1) in [9] by considering a simplified planar bi-dimensional model with a DEG power take-off shaped as a horizontal circular cylindrical shell segment and by neglecting the time-dependent response of practical dielectric elastomer materials; 2) in [12] by considering an ICD-DEG power take-off that is modeled as a perfect spherical shell segment and in which dielectric elastomer viscoelasticity is accounted via a quasi-linear formulation.

In this paper, a novel lumped-parameter dynamic model of ICD-DEGs (hereafter called reduced model) is introduced which also includes material viscoelasticity, gravity and inertia contributions. The model has been specifically developed for the techno-economic assessment, optimization and control of Poly-OWC systems. As compared to [12], the reduced model is obtained from a general energy balance (rather than from a local stress equilibrium at the ICD-DEG tip) and relies on a finite-deformation viscoelastic formulation [13,14]. First, the considered reduced model is described and validated via Finite Element Analysis (FEA). Second, a lumped-parameter model of

OWC hydrodynamics is introduced and coupled to the reduced model of the ICD-DEG. Third, the resulting fluido-electro-elastic wave-to-wire model (i.e. a model that makes it possible to predict electrical power production for given sea states) is used in a simulation case-study to evaluate the potential performances of a realistic OWC equipped with an ICD-DEG power take-off. Model validation and simulation case-study highlight that the proposed reduced method can be an adequately accurate and a computationally faster alternative to available continuum models [6] in applications such as preliminary assessment of ICD-DEG designs, as well as model-based ICD-DEG control and hardware in the loop simulations. The case-study also confirms that the energy harvesting performances of ICD-DEGs are suitable for OWC wave energy converters.

MODEL FOR INFLATED CIRCULAR DIAPHRAGM DIELECTRIC ELASTOMER GENERATORS

An ICD-DEG is depicted in Figure 2. It consists of an equi-biaxially pre-stretched planar circular dielectric elastomer membrane that is clamped along its perimeter at radius e and with thickness t (whereas e_0 and t_0 indicate the radius and thickness of the dielectric elastomer membrane in its planar undeformed state). When the opposing sides of the ICD-DEG are subjected to a differential pressure, p, and to an electric potential difference, V, the ICD-DEG undergoes an out of plane axial-symmetric (bubble-like) deformation (area expansion). In Figure 2(c), h identifies the resultant displacement of the ICD-DEG tip.

This section presents: 1) the general continuum model of ICD-DEGs, which involves solution of partial differential equations and which is not suited for real-time applications; 2) a reduced one-

degree-of-freedom model of ICD-DEGs, which can be used for fast design optimization, hardware-in-the-loop simulation and control; 3) the validation of the reduced model via FEA.

Continuum Model

Continuum models for the bubble-like electro-elastic deformations of axial-symmetric dielectric elastomer membranes have been proposed in [6, 15, 16]. They rely on the finite deformation formulation for incompressible hyper-elastic shells proposed by Adkins and Rivlin [17], and employ a free-energy function that includes the electrostatic energy stored in the dielectric elastomer material in addition to the standard strain-energy function term. Referring to Figure 2(a), let $\bar{r}$ indicate the radial position of the infinitesimal element of the undeformed ICD-DEG, with $\mathrm{d}\bar{r}$ indicating its longitudinal length. Upon bubble-like deformation (area expansion, see Figure 2(b-d)), this infinitesimal element varies its longitudinal length to $\mathrm{d}s$ and moves to a new configuration which is characterized by the radial distance r from the axis of symmetry, by the altitude z from a reference plane orthogonal to the axis of symmetry (here the plane containing the ICD-DEG clamping circle is taken as reference), and by the principal radii of curvature R_1 and R_2 (R_1 being in the meridian plane). For kinematic compatibility, Codazzi's equations impose [17]

$$\frac{r}{R_1 R_2}\left(\frac{\mathrm{d}s}{\mathrm{d}r}\right)^3 = \frac{\mathrm{d}^2 s}{\mathrm{d}r^2} \ \text{ and } \ \frac{\mathrm{d}}{\mathrm{d}r}\left(\frac{r}{R_2}\right) = \frac{1}{R_1} \ , \tag{1.1}$$

with

$$R_2 = -r \frac{\mathrm{d}s}{\mathrm{d}z} \quad \text{and} \quad \mathrm{d}s = \sqrt{\mathrm{d}r^2 + \mathrm{d}z^2} \,. \tag{1.2}$$

In this setting, ICD-DEG deformations are described by the following principal stretches

$$\lambda_1 = \frac{\mathrm{d}s}{\mathrm{d}\bar{r}} = \frac{\sqrt{\mathrm{d}r^2 + \mathrm{d}z^2}}{\mathrm{d}\bar{r}}, \quad \lambda_2 = \frac{r}{\bar{r}} \quad \text{and} \quad \lambda_3 = \lambda_1^{-1}\lambda_2^{-1}, \tag{2}$$

with λ_1 and λ_2 being in the longitudinal and latitudinal directions respectively. The third of equations (2) imposes the material incompressibility condition. In addition, balance of momentum yields [17]

$$\frac{\mathrm{d}N_1}{\mathrm{d}r} = \frac{N_2 - N_1}{r} - T \frac{\mathrm{d}s}{\mathrm{d}r} \quad \text{and} \quad \frac{N_1}{R_1} + \frac{N_2}{R_2} = P \,, \tag{3}$$

where P and T are the externally applied forces (per unit area of the membrane element) respectively acting along the normal and the tangent to the longitudinal direction of the infinitesimal ICD-DEG element, whereas N_1 and N_2 are the membrane forces (per unit length of longitudinal and latitudinal length). For the dynamic case, P and T account not only for the inflating pressure, p, but also for the gravitational and inertia forces acting on the ICD-DEG. Forces N_1 and N_2 are functions of the membrane principal stresses σ_1 and σ_2, namely

$$N_1 = t_0 \lambda_3 \sigma_1 \quad \text{and} \quad N_2 = t_0 \lambda_3 \sigma_2 \,, \tag{4.1}$$

$$\sigma_1 = \lambda_1 \frac{\partial \Psi}{\partial \lambda_1} \text{ and } \sigma_2 = \lambda_2 \frac{\partial \Psi}{\partial \lambda_2},$$

(4.2)

where Ψ is the free-energy density that accounts for the specific constitutive behavior of the considered material.

Based on equations (1-4) and by making T and P explicit in terms of pressure, gravity and inertia contributions, the balance of momentum for the ICD-DEG can be rewritten as the following system of Partial Differential Equations (PDE)

$$\begin{cases} \rho r \dfrac{\partial^2 r}{\partial \tau^2} = \dfrac{\partial}{\partial \bar{r}} \left(\dfrac{r \sigma_1}{\lambda_1^2} \dfrac{\partial r}{\partial \bar{r}} \right) - \dfrac{r \lambda_2 p}{t_0} \dfrac{\partial z}{\partial \bar{r}} - \dfrac{\sigma_2}{\lambda_2} \\[4mm] \rho r \dfrac{\partial^2 z}{\partial \tau^2} = \dfrac{\partial}{\partial \bar{r}} \left(\dfrac{r \sigma_1}{\lambda_1^2} \dfrac{\partial z}{\partial \bar{r}} \right) + \dfrac{r \lambda_2 p}{t_0} \dfrac{\partial r}{\partial \bar{r}} - \rho g r \end{cases},$$

(5.1)

where $\bar{r}$ and τ (time) are the independent variables, $r(\bar{r}, \tau)$ and $z(\bar{r}, \tau)$ are dependent variables, p is the pressure difference acting on the ICD-DEG, ρ is the density of the dielectric elastomer material and g is the acceleration of gravity, and with the following associated boundary and initial conditions

$$\begin{cases} r(e_0, \tau) = e, \ r(0, \tau) = 0, \ z(e_0, \tau) = 0, \ \dfrac{\partial z}{\partial \bar{r}}(0, \tau) = 0 \\[3mm] z(\bar{r}, 0) = 0, \ r(\bar{r}, 0) = e\bar{r}/e_0 \end{cases},$$

(5.2)

Under the hypothesis of linear strain-independent dielectric properties [18], the free-energy density of DEs can be decomposed as

$$\Psi = \Psi_{st} - \Psi_{es} \quad \text{with} \quad \Psi_{es} = \frac{1}{2}\varepsilon\lambda_1^2\lambda_2^2\left(\frac{V}{t_0}\right)^2, \tag{6}$$

where Ψ_{st} is a suitable strain energy function, and Ψ_{es} is the electrostatic energy density, with ε and V respectively being the dielectric constant of the considered dielectric elastomer material and the electric potential difference acting between the ICD-DEG electrodes. As regards Ψ_{st}, assuming a standard visco-hyperlesatic response for the considered dielectric elastomer material [13, 14], which is represented by a Zener model with two hyper-elastic networks and one dashpot (see Figure 3), and assuming the Gent's form for both hyper-elastic networks [19], a suitable expression for the strain energy function to be used in (6) reads as [13, 14]

$$\Psi_{st} = -\frac{\mu_1 J_1}{2}\log\left(1 - \frac{\lambda_1^2 + \lambda_2^2 + \lambda_1^{-2}\lambda_2^{-2} - 3}{J_1}\right) - \frac{\mu_2 J_2}{2}\log\left(1 - \frac{\lambda_1^2\lambda_{1,v}^{-2} + \lambda_2^2\lambda_{2,v}^{-2} + \lambda_{1,v}^2\lambda_{2,v}^2\lambda_1^{-2}\lambda_2^{-2} - 3}{J_2}\right), \tag{7}$$

where the material parameters μ_1, μ_2, J_1 and J_2 are the shear moduli and the constants related to the limiting first-stretch-invariants of the two hyper-elastic networks, whereas $\lambda_{1,v}$ and $\lambda_{2,v}$ are additional internal variables that are associated to the viscous motion of the material and dependent on $\bar{r}$ and τ (namely, $\lambda_{1,v}(\bar{r},\tau)$ and $\lambda_{2,v}(\bar{r},\tau)$).

On account of equations (4.2) and (7), the ICD-DEG principal stresses read as

$$\sigma_1 = \sigma_{1,eq} + \sigma_{1,neq} - \sigma_{es} \text{ and } \sigma_2 = \sigma_{2,eq} + \sigma_{2,neq} - \sigma_{es}, \tag{8.1}$$

with

$$\sigma_{es} = \varepsilon \lambda_1^2 \lambda_2^2 \left(\frac{V}{t_0} \right)^2, \tag{8.2}$$

$$\sigma_{eq,1} = \frac{\mu_1 J_1 \left(\lambda_1^2 - \lambda_1^{-2} \lambda_2^{-2} \right)}{J_1 - \lambda_1^2 - \lambda_2^2 - \lambda_1^{-2} \lambda_2^{-2} + 3} \text{ and } \sigma_{neq,1} = \frac{\mu_2 J_2 \left(\lambda_1^2 \lambda_{1,v}^{-2} - \lambda_{1,v}^2 \lambda_{2,v}^2 \lambda_1^{-2} \lambda_2^{-2} \right)}{J_2 - \lambda_1^2 \lambda_{1,v}^{-2} - \lambda_2^2 \lambda_{2,v}^{-2} - \lambda_{1,v}^2 \lambda_{2,v}^2 \lambda_1^{-2} \lambda_2^{-2} + 3}, \tag{8.3}$$

$$\sigma_{eq,2} = \frac{\mu_2 J_2 \left(\lambda_2^2 - \lambda_1^{-2} \lambda_2^{-2} \right)}{J_2 - \lambda_1^2 - \lambda_2^2 - \lambda_1^{-2} \lambda_2^{-2} + 3} \text{ and } \sigma_{neq,2} = \frac{\mu_2 J_2 \left(\lambda_2^2 \lambda_{2,v}^{-2} - \lambda_{1,v}^2 \lambda_{2,v}^2 \lambda_1^{-2} \lambda_2^{-2} \right)}{J_2 - \lambda_1^2 \lambda_{1,v}^{-2} - \lambda_2^2 \lambda_{2,v}^{-2} - \lambda_{1,v}^2 \lambda_{2,v}^2 \lambda_1^{-2} \lambda_2^{-2} + 3}. \tag{8.4}$$

As regards the internal variables, according to [13, 14], the time evolution of $\lambda_{1,v}$ and $\lambda_{2,v}$ is assumed to be governed by the following dynamic constitutive relations

$$\frac{d\lambda_{1,v}}{d\tau} = \frac{2\sigma_{1,neq} - \sigma_{2,neq}}{6\varsigma\mu_2} \lambda_{1,v} \text{ and } \frac{d\lambda_{2,v}}{d\tau} = \frac{2\sigma_{2,neq} - \sigma_{1,neq}}{6\varsigma\mu_2} \lambda_{2,v}, \tag{9.1}$$

where the parameter ς is the relaxation time of the material, with the following initial conditions

$$\lambda_{1,v}\left(\bar{r},0\right)=\lambda_1\left(\bar{r},0\right) \text{ and } \lambda_{2,v}\left(\bar{r},0\right)=\lambda_2\left(\bar{r},0\right). \tag{9.2}$$

The continuum model represented by equations (1)-(4), (8) and (9) governs the dynamic response of ICD-DEGs. It can be considered as the integration of the dynamic electro-hyperelastic model described in [20] with the quasi-static electro-visco-hyperelastic model described in [6], but formulated with r and z as dependent displacement field variables. Since fast solution of this partial differential equation problem can be difficult to achieve, a reduced but yet accurate real-time model for ICD-DEGs is required in many practical contexts.

Reduced Model

In this subsection, the continuum electro-visco-elastic model of the ICD-DEG that has been described above is reduced to a lumped parameter model with one single kinematic degree of freedom. The reduced model is based on the following simplifying assumptions:

- the ICD-DEG deforms as a perfect spherical cap with tip height h and radius R;
- ICD-DEG deformation is prevalently equi-biaxial, with the amount of deformation depending on h and varying with the radial distance r (or equivalently with $\bar{r}$);
- ICD-DEG capacitance is assumed to be equivalent to that of a planar circular capacitor with variable thickness;
- the visco-elastic response of the ICD-DEG is represented via a Zener model with a first hyper-elastic network subjected to non-homogeneous equi-biaxial deformations (depending on both h and $\bar{r}$), which makes it possible to capture the global equilibrium response of the ICD-DEG

with good accuracy, and a second hyper-elastic network together with a dashpot element both subjected to piecewise homogeneous equi-biaxial deformations (depending on h only), which provides a good approximation of the global non-equilibrium response of the ICD-DEG.

The first three assumptions have already been demonstrated to provide sufficiently accurate models for the electro-elastic response of pre-stretched ICD-DEGs featuring limited mass density ($\rho \approx 1000$ kg·m^{-3}), and working in the range $|h| < e$ with limited accelerations ($|\ddot{h}| < g$, with $g = 9.8$ m·s^{-2}) [12].

The variable h is taken as the kinematic variable univocally describing the geometric configuration of the ICD-DEG. According to the first assumption, equations (1.1) are identically satisfied. Moreover, according to Figure 2(c), the following relations hold

$$R_1 = R_2 = R \text{, where } R = \frac{h^2 + e^2}{2h}, \tag{10}$$

$$ds = Rd\vartheta, \quad r = R\sin\vartheta, \quad dr = R\cos\vartheta\, d\vartheta, \tag{11}$$

$$\lambda_1 = R\frac{d\vartheta}{d\bar{r}}, \quad \lambda_2 = R\frac{\sin\vartheta}{\bar{r}}, \tag{12}$$

where ϑ is the zenith angle indicating the location of the deformed ICD-DEG element ds along the longitudinal direction.

According to the second assumption, to the first-order of approximation, equations (12) reduce to

$$\lambda = R\frac{\mathrm{d}\vartheta}{\mathrm{d}\bar{r}} = R\frac{\sin\vartheta}{\bar{r}}\,, \tag{13}$$

which, upon solution of the last equality, yields

$$\vartheta(h,\bar{r}) = 2\mathrm{atan}\left(\frac{h\bar{r}}{ee_0}\right), \tag{14}$$

$$\lambda(h,\bar{r}) = ee_0\left(h^2 + e^2\right)\Big/\left(e^2 e_0^2 + h^2 \bar{r}^2\right), \tag{15}$$

thereby providing the expression of the prevalent equi-biaxial stretch, λ, as function of the ICD-DEG height h and undeformed radial distance $\bar{r}$.

Given (15), the radial and vertical positions of the deformed ICD-DEG element $\mathrm{d}s$ can be expressed as

$$r = R\sin\vartheta = \lambda\bar{r} = \frac{ee_0\left(h^2 + e^2\right)\bar{r}}{\left(e^2 e_0^2 + h^2 \bar{r}^2\right)}\,, \tag{16.1}$$

$$z = \sqrt{R^2 - r^2} - R + h = \frac{e^2\left(e_0^2 - \bar{r}^2\right)h}{\left(e^2 e_0^2 + h^2 \bar{r}^2\right)}\,. \tag{16.2}$$

Based on the kinematic constrains described by relations (10)-(15), the reduced equation of motion for the ICD-DEG can be obtained from the following energy inequality

$$\frac{\mathrm{d}}{\mathrm{d}\tau}\left(\mathcal{K}+\mathcal{U}_g+\mathcal{U}_{me}+\mathcal{U}_{el}\right)-W_{me}-W_{el}\leq 0, \tag{17}$$

where $\mathcal{K}$ and $\mathcal{U}_g$ are the kinetic energy and gravitational potential associated to the density ρ of the ICD-DEG, namely

$$\mathcal{K}=\int_0^{R\arcsin(e/R)}\pi\rho\left[\left(\frac{\mathrm{d}r}{\mathrm{d}\tau}\right)^2+\left(\frac{\mathrm{d}z}{\mathrm{d}\tau}\right)^2\right]tr\mathrm{d}s=\pi\rho t_0\int_0^{e_0}\left[\left(\frac{\mathrm{d}r}{\mathrm{d}\tau}\right)^2+\left(\frac{\mathrm{d}z}{\mathrm{d}\tau}\right)^2\right]\bar{r}\mathrm{d}\bar{r}, \tag{18}$$

$$\mathcal{U}_g=\int_0^{R\arcsin(e/R)}2\pi\rho gztr\mathrm{d}s=2\pi\rho gt_0\int_0^{e_0}z\bar{r}\mathrm{d}\bar{r}; \tag{19}$$

$\mathcal{U}_{el}$ is the electric potential energy stored in the ICD-DEG, namely

$$\mathcal{U}_{el}=\int_0^{R\arcsin(e/R)}2\pi\left(\frac{1}{2}\varepsilon E^2\right)tr\mathrm{d}s=\frac{1}{2}CV^2, \tag{20}$$

with C being the ICD-DEG capacitance

$$C(h) = \int_0^{R\arcsin(e/R)} \varepsilon \frac{2\pi r}{t} \mathrm{d}s = \frac{\pi \varepsilon e e_0}{3 t_0} \lambda_{\mathrm{T}} \left(\lambda_{\mathrm{T}}^2 + \frac{e}{e_0} \lambda_{\mathrm{T}} + \frac{e^2}{e_0^2} \right),$$ (21)

which, according to the third assumption, is only dependent on the maximum prevalent equi-biaxial stretch λ_{T} (occurring at the ICD-DEG tip) that is defined as

$$\lambda_{\mathrm{T}}(h,0) = \left(h^2 + e^2 \right) / \left(e e_0 \right);$$ (22)

W_{me} is the mechanical power provided by the pressure difference p on the ICD-DEG, namely

$$W_{me} = p \dot{\Omega}_{\mathrm{G}},$$ (23)

with Ω_{G} being the volume subtended by the ICD-DEG

$$\Omega_{\mathrm{G}} = \frac{\pi h}{6} \left(3 e^2 + h^2 \right);$$ (24)

W_{el} is the electrical power provided by an external energy circuit on the ICD-DEG, namely

$$W_{el} = V \dot{Q},$$ (25)

with Q being the electric charge residing on the ICD-DEG electrodes

$$Q = CV \; ; \tag{26}$$

and $\mathcal{U}_{me}$ is the elastic potential energy stored in the ICD-DEG, namely

$$\mathcal{U}_{me} = \int_{0}^{R\arcsin(e/R)} 2\pi\Psi_{st}(\lambda)\, tr\, \mathrm{d}s = 2\pi t_0 \int_{0}^{e_0} \Psi_{st}(\lambda)\, \bar{r}\, \mathrm{d}\bar{r} \;, \tag{27}$$

with Ψ_{st} being the reduced strain energy function

$$\Psi_{st} = -\frac{\mu_1 J_1}{2}\log\left(1 - \frac{2\lambda^2 + \lambda^{-4} - 3}{J_1}\right) - \sum_{i=1}^{n}\left[\frac{\mu_2 J_2}{2}\log\left(1 - \frac{2\lambda_{i,*}^2\lambda_{i,v}^{-2} + \lambda_{i,v}^4\lambda_{i,*}^{-4} - 3}{J_2}\right)\left(u(\bar{r} - \bar{r}_{i-1}) - u(\bar{r} - \bar{r}_i)\right)\right], \tag{28}$$

where $u(\bullet)$ is the Heaviside unit step function with $\bar{r}_i = i\, e_0/n$. According to the fourth assumption, Ψ_{st} comprises a first hyper-elastic term, which accounts for the non-homogeneous equilibrium response of the ICD-DEG, and a second hyper-elastic term, which provides an estimate of the non-equilibrium response of the ICD-DEG. The first term depends on the prevalent equi-biaxial stretch λ that is function of both h and $\bar{r}$. The second term depends on piecewise constant elastic and viscous stretches $\lambda_{i,*}$ and $\lambda_{i,v}$ (for $i = 1,\ldots,n$) that can be defined at given points $\bar{r} = r_{i,*}$ of the ICD-DEG (with the choices $r_{i,*} = \bar{r}_{i-1}$, $r_{i,*} = \bar{r}_i$ and $r_{i,*} = 0.5(\bar{r}_{i-1} + \bar{r}_i)$ respectively giving an upper, lower and intermediate

estimate of the non-equilibrium response). The number n is an integer whose choice depends on the level of accuracy required for the non-equilibrium response. Once the n specific values for $r_{i,*}$ are chosen, the elastic stretches $\lambda_{i,*}$ are only a function of the kinematic variable h, namely

$$\lambda_{i,*}\left(h,r_{i,*}\right) = ee_0\left(h^2 + e^2\right)\big/\left(e^2 e_0^2 + h^2 r_{i,*}^2\right), \tag{29}$$

whereas the viscous stretches $\lambda_{i,v}$ are internal variables acting as additional unknowns for which an appropriate constitutive equation needs to be provided.

By considering h, $\lambda_{i,v}$ and V as independent variables, satisfaction of the energy inequality (17) provides the following relations

$$\ddot{h}\frac{\partial}{\partial\dot{h}}\left(\mathcal{K}\right) + \dot{h}\frac{\partial}{\partial h}\left(\mathcal{K} + \mathcal{U}_g + \mathcal{U}_{me}\right) - \dot{h}p\frac{\partial}{\partial h}\left(\Omega_G\right) = \dot{h}\frac{V^2}{2}\frac{\partial}{\partial h}\left(C\right), \tag{30}$$

$$\frac{\partial\Psi_{st}}{\partial\lambda_{i,v}}\dot{\lambda}_{i,v} \leq 0, \quad \text{for } i = 1,\ldots,n. \tag{31}$$

Equation (30) describes the dynamic response of the ICD-DEG and can be written in the following lumped-parameter form

$$\ddot{h} = \frac{p + \Lambda\left(h\right)V^2 - B\left(h\right)\dot{h}^2 - \displaystyle\sum_{i=1}^{n}K_i\left(h,\lambda_{i,v}\right)h}{M\left(h\right)}, \tag{32}$$

where the variable coefficients $\Lambda(h)$, $B(h)$, $K_i(h, \lambda_{i,v})$ and $M(h)$ can be expressed in closed form upon manipulation of equations (17)-(29).

Equation (31) provides a thermodynamic requirement for the constitutive relation that regulates the evolution in time of the internal variables $\lambda_{i,v}$. Similar to (9.1), the following constitutive equations are chosen

$$\frac{\mathrm{d}\lambda_{i,v}}{\mathrm{d}\tau} = \frac{J_2}{6\varsigma}\left(\frac{\lambda_{i,*}^2 \lambda_{i,v}^{-2} - \lambda_{i,v}^4 \lambda_{i,*}^{-4}}{J_2 - 2\lambda_{i,*}^2 \lambda_{i,v}^{-2} - \lambda_{i,v}^4 \lambda_{i,*}^{-4} + 3}\right)\lambda_{i,v} \quad \text{for } i = 1,...,n , \tag{33}$$

which readily satisfy relations (31).

The differential equations (32) and (33) make it possible to study the time evolution of the ICD-DEG tip height h as function of the time-varying pressure p and voltage V. During this motion, the electrical power that the ICD-DEG can exchange with the outer electric circuit is given by the last term of equation (30), with negative (positive) sign indicating that electric power is produced (spent) by the ICD-DEG.

To harvest energy out from the deformation of the ICD-DEG, the voltage across the ICD-DEG electrodes needs to be properly regulated. Here, a control law with energy generation at maximum electric field is considered ([2,3], see Figure 4), which features a cyclical series of electromechanical transformations: 1) at zero electric field ($V = 0$), in which the ICD-DEG is made expand in area from $\lambda_{\mathrm{T,low}}$ to $\lambda_{\mathrm{T,high}}$ (with $\lambda_{\mathrm{T,low}} < \lambda_{\mathrm{T,high}} < \lambda_{\mathrm{BD}}$, where λ_{BD} is the maximum stretch that can be sustained by the

dielectric elastomer material); 2) at constant deformation ($\lambda_\mathrm{T} = \lambda_\mathrm{T,high}$), in which the ICD-DEG is

charged from zero up to the maximum electric field E_BD (where E_BD is close to the dielectric strength

of the considered dielectric elastomer material and may depend on the stretch λ_T, namely $E_\mathrm{BD}(\lambda_\mathrm{T})$

[3]); 3) at maximum electric field ($V = E_\mathrm{BD}t_0\lambda_\mathrm{T}^{-2}$), in which the ICD-DEG is made contract in area from

$\lambda_\mathrm{T,high}$ to $\lambda_\mathrm{T,low}$; and 4) at constant deformation ($\lambda_\mathrm{T} = \lambda_\mathrm{T,low}$), in which the ICD-DEG is discharged from

E_BD down to zero electric field ($V = 0$). Note that for $h \neq 0$, the electric field acting across the ICD-

DEG is not uniform. For any given V, the considered value of $V\lambda_\mathrm{T}^2/t_0$ is the maximum electric field

acting on the ICD-DEG, which occurs at its axis of symmetry.

Based on the last term of equation (30) and on the chosen harvesting control law (Figure 4),

the electric power, W, and the energy per cycle, U_{cycle}, that can be generated by the ICD-DEG are

$$W = \dot{h}\frac{V2}{2}\frac{\partial}{\partial h}(C) = \dot{\lambda}_\mathrm{T}\frac{V2}{2}\frac{\partial}{\partial \lambda_\mathrm{T}}(C) = \frac{\pi\varepsilon ee_0t_0}{6}\left[E_\mathrm{BD}(\lambda_\mathrm{T})\right]^2\left(3\lambda_\mathrm{T}^{-2} + 2\frac{e}{e_0}\lambda_\mathrm{T}^{-3} + \frac{e2}{e_0^2}\lambda_\mathrm{T}^{-4}\right)\dot{\lambda}_\mathrm{T}, \tag{34}$$

$$U_{cycle} = \int_{\lambda_\mathrm{T,high}}^{\lambda_\mathrm{T,low}} \frac{V2}{2}\frac{\partial}{\partial \lambda_\mathrm{T}}(C)\mathrm{d}\lambda_\mathrm{T} = \frac{\pi\varepsilon ee_0t_0}{6}\int_{\lambda_\mathrm{T,high}}^{\lambda_\mathrm{T,low}}\left[E_\mathrm{BD}(\lambda_\mathrm{T})\right]^2\left(3\lambda_\mathrm{T}^{-2} + 2\frac{e}{e_0}\lambda_\mathrm{T}^{-3} + \frac{e2}{e_0^2}\lambda_\mathrm{T}^{-4}\right)\mathrm{d}\lambda_\mathrm{T}. \tag{35}$$

Model Validation

In this section, the reduced model of the ICD-DEG given by equations (32) and (33) is

validated with respect to the continuum model expressed by equations (5), (8) and (9).

Validation is performed by considering an ICD-DEG power take-off for a realistic OWC (like the Pico plant in the Azores [21]). The considered ICD-DEG is made of a commercial dielectric elastomer material (VHB-4910 by 3M [14]), with $\rho = 960$ kgm^{-3}, $\mu_1 = 18$ kPa, $J_1 = 110$, $\mu_2 = 42$ kPa, $J_2 = 55$ and $\varsigma = 400$ s, $\varepsilon = 4.5 \cdot 8.8\mathrm{e}^{-12}$ F/m, and having the following geometrical dimensions: $e = 5$ m, $t = 0.1$ m and $e_0 = 2$ m. A dynamic case is studied where the ICD-DEG is subjected to gravity, to a constant voltage $V = 2.5$ MV (which has been chosen to provide the ICD-DEG with a maximum electric field of about 100 MVm^{-1} that is compatible with the electric breakdown strength of the considered material), and to a differential pressure p varying sinusoidally with 4.25 kPa amplitude and 0.1Hz frequency (that is compatible to typical wave energy harvesting applications).

The continuum model is implemented in the FEA software Comsol Multiphysics using the time-dependent PDE application mode in one dimension, with the ICD-DEG discretized in 20 equal elements with Lagrange quadratic shape functions (for a total of 164 degrees of freedom), and solved with the Backward Differentiation Formula (BDF) method with 0.02 s time steps. Number of elements and solution time steps have been chosen so as to maximize accuracy and minimize solution time (specifically, the use of less elements and larger time steps did not make the model converge to a solution, whereas the use of more elements and smaller time steps did not substantially increase solution accuracy).

The reduced model is implemented in Matlab Simulink and solved, for different values of n (n = 1, 3, 5, 10) and with $r_{i,*} = 0.5(\bar{r}_{i-1} + \bar{r}_i)$, by means of the ODE 45 method with variable time steps. Values of n above 10 have not been considered since they do not provide any substantial improvement in the accuracy of the model and only increase computation time. A simulation time of 2000 s has been considered for both models.

Figure 5 reports the comparison between the time evolution of the ICD-DEG tip height predicted by the reduced model (lines) and by FEA (markers). As shown, the response predicted by the reduced model matches very well that of the FEA model with an error that is lower than 10% for $n \geq 5$.

In terms of computational complexity, the time required on an Intel Core i7-4500U (1.80GHz with 8GB of RAM) to perform 2000 s of simulation is 3.1 s, 4.5 s, 5.6 s and 8.6 s for the reduced model with $n = 1$, $n = 3$, $n = 5$ and $n = 10$, and 854 s for the FEA model.

As such, under the hypotheses mentioned above, the reduced model proves very effective for the preliminary assessment of ICD-DEG designs and for real-time applications.

POLYMERIC OSCILLATING WATER COLUMN MODEL

Investigating the performances of ICD-DEG power take-off systems into Poly-OWCs (like the one depicted in Figure 1) requires to couple the reduced electro-elastic model described by equations (32), (33) and (35) with a suitable hydrodynamic model that is capable of representing the oscillatory response of the water column to both the excitation pressure p_E, which is due to the water wave field, and the air-chamber pressure p_C, which also acts on the ICD-DEG (namely, $p = p_C - p_{atm}$, where p_{atm} is the atmospheric pressure).

Similarly to a previous study [9], a lumped-parameter hydrodynamic model of an ideal OWC system is considered here. With reference to Figure 1, the system comprises a fixed cuboid OWC structure opened to a wave basin of semi-infinite extension and constant depth. Introducing the spatial horizontal and vertical coordinates x, y and z (z being positive when pointing up-ward), the wave basin extends from $-\infty \leq x \leq 0$ and $-\infty \leq y \leq \infty$, and has a depth equal to b. The OWC structure has a square

cross section, with edge equal to c, and is opened to the wave basin on its front-wall (at $x = 0$), with the submersed aperture being defined by the constant distance a measured from the Mean Water Level (MWL). The OWC air-chamber comprises a cuboid part, which extends by the constant length d from the MWL, plus (or minus) the spherical segment with height h that is subtended by the ICD-DEG.

Beside the specific OWC geometry, the considered lumped-parameter hydrodynamic model relies on the following assumptions:

- ideal fluid and linear water-wave theory;

- harmonic monochromatic waves on water of constant depth;

- perfect wave reflection from the OWC front-wall;

- no disturbance (for instance radiation) is caused by the OWC to the outer wave field;

- the free-water surface inside the OWC is replaced by a weightless rigid piston, whose motion with respect to the MWL can be described by the single displacement variable η;

- adiabatic compression-expansion of the air entrapped between the free-water surface of the column and the ICD-DEG.

With these simplifications, the equation of motion of the column of water oscillating within the hollow structure follows as [9]

$$\ddot{\eta} = \frac{p_{\text{atm}} + p_{\text{E}}(\tau) - p_{\text{C}}(\tau) - \rho_w g \eta - D_1 \dot{\eta}}{\rho_w (a + \eta)}, \tag{36}$$

where ρ_w is the constant water density, D_1 is a linear damping coefficient that accounts for the hydraulic losses occurring within the OWC duct, and where the pressures p_{C} and p_{E} take the forms

$$p_C(\tau) = p_C(\eta, h) = C_0 \left[\Omega_C(\eta, h) \right]^{-\gamma}, \tag{37}$$

with γ being the adiabatic compression-expansion index for air ($\gamma = 1.4$), C_0 being a constant that sets the steady condition of the air-chamber (pressurized, depressurized, or at atmospheric pressure) and Ω_C being the air-chamber volume

$$\Omega_C(\eta, h) = c^2(d - \eta) + \Omega_G, \tag{38}$$

and

$$p_E = \frac{\rho_w g H_s}{(b-a)\sqrt{2}} \frac{\sinh\left[K(b-a)\right]}{K \cosh(Kb)} \cos\left(\frac{2\pi}{T}\tau\right), \tag{39}$$

with H_s and T being the significant height and period of the incident wave, and K being the angular repetency of the propagating wave (also called wave number) that is obtained by the solution of the dispersion relation

$$K \tanh(Kb) = \frac{1}{g}\left(\frac{2\pi}{T}\right)^2. \tag{40}$$

Equations (36)-(40), together with (32)-(33) and (35), provide a fully coupled fluido-electro-elastic wave-to-wire model for the Poly-OWC equipped with an ICD-DEG power take-off system.

SIMULATION RESULTS

The fluido-electro-elastic wave-to-wire model, which has been described in the previous sections, is used here to investigate the influence of design parameters and of variable sea-state conditions on the energy that can be harvested by a Poly-OWC equipped with an ICD-DEG power take-off system.

The reported results have been obtained via the numerical solution of equations (32)-(33) and (36)-(40) in Matlab Simulink; specifically for an OWC with dimensions: $a = 6$ m, $b = 8$ m, $c = 12$ m and $d = 7.29$ m (these dimensions resemble those of the Pico plant installed at the Azores [21]), and with an ICD-DEG power take-off (employing VHB-4910 by 3M as dielectric elastomer material) featuring $e = 5$ m, $\rho = 960$ kgm^{-3}, $\mu_1 = 18$ kPa, $J_1 = 110$, $\mu_2 = 42$ kPa, $J_2 = 55$ and $\varsigma = 400$ s, $\varepsilon = 4.5 \cdot 8.8\mathrm{e}^{-12}$ F/m, $\lambda_{BD} = 7$, $E_{BD} = 30\ \lambda^{1.13}$ MVm^{-1} [3], $n = 5$, $r_{i,*} = 0.5(\bar{r}_{i-1} + \bar{r}_i)$. The considered material parameters are taken from [14]. These values provide a less dissipative material response as compared to the quasi-linear viscoelastic model that was assumed in [12].

The influence of design parameters on the energy harvesting performances of the Poly-OWC system is described in Figure 6, which reports U_{cycle} as function of the ICD-DEG pre-stretch $\lambda_\mathrm{p} = e/e_0$ and of the steady state tip height h_0 (i.e. the height with no incident wave field, with h_0 being positive or negative depending on whether the air-chamber is pressurized or depressurized). Results are obtained for a monochromatic wave with $H_s = 2.9$ m and $T = 11.5$ s. Different figures are for different thicknesses, namely $t = 0.05$ m, $t = 0.2$ m and $t = 0.3$ m (with t being measured at $h = 0$). As shown,

increasing values of membrane thickness make the energy productivity larger. Indeed, too small values of t (for instance $t = 0.05$ m) are not able to sustain the OWC chamber pressures induced by ocean waves (especially for the larger values of λ_p and h_0). Of course, too large values of t will make the membrane too stiff, thereby excessively limiting ICD-DEG deformation (and thus energy conversion capabilities).

The influence of variable sea-state conditions on the energy harvesting performances is described in Figure 7, which reports U_{cycle} for different Poly-OWC systems equipped with ICD-DEGs having identical thickness ($t = 0.1$ m, measured at $h = 0$), but different pre-stretches $\lambda_p = e/e_0$ and steady state tip heights h_0, and subjected to the following nine sea-state conditions: $H_s = 0.8$ m and $T = 9$ s; $H_s = 1.2$ m and $T = 9.5$ s; $H_s = 1.6$ m and $T = 10$ s; $H_s = 2$ m and $T = 10.5$ s; $H_s = 2.4$ m and $T = 11$ s; $H_s = 2.9$ m and $T = 11.5$ s; $H_s = 3.4$ m and $T = 12$ s; $H_s = 4$ m and $T = 12.5$ s; $H_s = 4.5$ m and $T = 13$ s (these are the nine sea-states characterizing the wave climate at the Pico plant in the Azores [21]). As shown, the energy harvesting performances of the Poly-OWC increase as the sea state becomes more energetic.

All the plots reported in Figures 6 and 7 are rather specular with respect to $h_0 = 0$, indicating that OWC chamber pressurization ($h_0 > 0$) and depressurization ($h_0 < 0$) almost provide the same effects. Except for the cases where the ICD-DEG is undersized with respect to the energy content of the sea state, the maximal energy harvesting performance of the Poly-OWC occurs for values of h_0 that are different than zero and whose magnitude decreases as the sea state becomes more energetic. As expected, an optimal value for λ_p exists for different values of ICD-DEG thickness and sea state condition; for the considered cases, this optimum lies within the range 2.5 and 3.5.

The sensitivity of Poly-OWC energy productivity on h_0 increases as λ_p gets closer to its optimum value, as t decreases, and as the sea state becomes more energetic. The sensitivity of Poly-OWC energy productivity on λ_p decreases as h_0 goes away from its optimum value, as t increases and as the sea state becomes less energetic. For a given Poly-OWC system (with fixed t and λ_p) pressurization and depressurization of the OWC air chamber (that is, regulation of h_0) could be used to better tune the overall dynamic response of the Poly-OWC system to the different sea states so as to maximize energy production.

In terms of overall performances, the maximum average powers that could be harvested by the considered Poly-OWC device for each monochromatic sea-state are: 52 kW; 63 kW; 95 kW; 114 kW; 124 kW; 136 kW; 141 kW; 165 kW; 181 kW. These numbers compare already well with those estimated for the same OWC system equipped with a turbo-generator [22]. As expected, the reported values of energy productivity are significantly larger (20-30% more) than those presented in [12]. This is attributed to the less dissipative response of the ICD-DEG model considered here.

This confirms the viability and potentialities of the Poly-OWC concept, especially as better dielectric elastomer materials with lower dissipative effects and adequate fatigue and ageing resistance become available.

CONCLUSIONS

Inflated Circular Diaphragm Dielectric Elastomer Generators (ICD-DEGs) offer promising potentials as power take-off systems for Oscillating Water Column (OWC) wave energy converters. In this paper, a reduced, yet accurate, electro-visco-elastic model for ICD-DEGs has been presented. As compared to available continuum models valid for axial-symmetric Dielectric Elastomer

membranes, the proposed one does not involve the solution of computationally demanding partial differential equations, and thus can be more easily integrated into existing fast-running wave-to-wire models of OWC systems. Coupling of the proposed electro-visco-elastic model with a lumped-parameter model of the OWC hydrodynamics has also been described which provides an effective fluido-electro-elastic wave-to-wire model for fast design optimization, real-time control and hardware-in-the-loop simulation of realistic systems. A simulation case study has also been presented which shows how a wave-to-wire model of this kind can be used for the parametric analysis and design of OWCs equipped with an ICD-DEG power take-off.

ACKNOWLEDGMENT

REFERENCES

[1] Carpi, F., De Rossi, D., Kornbluh, R., Pelrine, R., and Sommer-Larsen, P., 2008, *Dielectric Elastomers as Electromechanical Transducers: Fundamentals, Materials, Devices, Models and Applications of an Emerging Electroactive Polymer Technology*, Elsevier.

[2] Pelrine, R., Kornbluh, R., Eckerle, J., Jeuck, P., Oh, S., Pei, Q., and Stanford, S., 2001, Dielectric elastomers: Generator mode fundamentals and applications, in *Proc. SPIE vol. 4329, Electroactive Polymer Actuators and Devices (EAPAD)*, pp. 148-156.

[3] Koh, S.J.A., Keplinger, C., Li, T., Bauer, S., and Suo, Z., 2011, Dielectric elastomer generators: How much energy can be converted?, *IEEE/ASME Transactions on Mechatronics*, **16**(1), pp. 33-41.

[4] McKay, T., O'Brien, B., Calius, E., and Anderson, I., 2010, Self-priming dielectric elastomer generators, *Smart Material and Structures*, **19**(5), pp. 055025.

[5] Jean-Mistral, C., Basrour, S, and Chaillout, J.-J., 2010, Modelling of dielectric polymers for energy scavenging applications, *Smart Material and Structures*, **19**(10), pp. 105006.

[6] Li, T., Qu, S., and Yang, W., 2012, Energy harvesting of dielectric elastomer generators concerning inhomogeneous fields and viscoelastic deformation, *Journal of Applied Physics*, **112**(3), pp. 034119.

[7] Chiba, S., Waki, M., Kornbluh, R., and Pelrine, R., 2008, Innovative power generators for energy harvesting using electroactive polymer artificial muscles, in *Proc. SPIE vol. 6927, Electroactive Polymer Actuators and Devices (EAPAD)*, pp. 692715.

[8] Jean, P., Wattez, A., Ardoise, G., Melis, C., Van Kessel, R., Fourmon, A., Barrabino, E., Heemskerk, J., and Queau, J.P., 2012, Standing wave tube electro active polymer wave energy converter, in *Proc. SPIE vol. 8340, Electroactive Polymer Actuators and Devices (EAPAD)*, pp. 83400C.

[9] Vertechy, R., Fontana, M., Rosati-Papini, G.P., and Bergamasco, M., 2013, Oscillating-water-column wave-energy-converter based on dielectric elastomer generator, in *Proc. SPIE vol. 8687, Electroactive Polymer Actuators and Devices (EAPAD)*, pp. 86870I.

[10] Scherber, B., Grauer, M., and Köllnberger, A., 2013, Electroactive polymers for gaining sea power, in *Proc. SPIE vol. 8687, Electroactive Polymer Actuators and Devices (EAPAD)*, pp. 86870K.

[11] Moretti, G., Forehand, D., Vertechy, R., Fontana, M., and Ingram, D., 2014, Modeling of a Surging Wave Energy Converter with Dielectric Elastomer Power Take-Off, in *Proc. of the ASME 2014 33rd International Conference on Ocean, Offshore and Arctic Engineering*, paper n. OMAE2014-23559, June 8-13, San Francisco.

[12] Rosati Papini, G.P. Vertechy, R., and Fontana, M., 2013, Dynamic Model of Dielectric Elastomer Diaphragm Generators for Oscillating Water Column Wave Energy Converters, in *Proc. of ASME 2013 Conference on Smart Materials, Adaptive Structures and Intelligent Systems*, paper n. SMASIS2013-3255, September 16-18, Snowbird (Utah).

[13] Govindjee, S., and Reese S., 1997, A presentation and comparison of two large deformation viscoelasticity models, *Journal of Engineering Materials and Technology*, **119**(3), pp. 251-255.

[14] Foo, C., Cai, S., Koh, A., Bauer, S., and Suo, Z., 2012, Model of dissipative dielectric elastomers, *Journal of Applied Physics*, **111**(3), pp. 034102.

[15] Goulbourne, N.C., Mockensturm, E., and Frecker, M., 2007, Electro-elastomers: Large deformation analysis of silicone membranes, *International Journal of Solids and Structures*, **44**(9), pp. 2609-2626.

[16] He, T., Zhao, X., and Suo, Z., 2009, Equilibrium and stability of dielectric elastomer membranes undergoing inhomogeneous deformation, *Journal of Applied Physics*, **106**, pp. 083522.

[17] Adkins, J.E., and Rivlin, R.S., 1952, Large Elastic Deformations of Isotropic Materials: IX The Deformation of Thin Shells, *Philosophical Transactions of the Royal Society of London. Series A, Mathematical and Physical Sciences*, **244**(888), pp. 505-531.

[18] Vertechy, R., Berselli, G., Parenti Castelli, V., and Bergamasco, M., 2013, Continuum thermo-electro-mechanical model for electrostrictive elastomers, *Journal of Intelligent Material Systems and Structures*, **24**(6), pp. 761-778.

[19] Gent, A.N., 1996, A new constitutive relation for rubber, *Rubber Chemistry and Technology*, **69**(1), pp. 59-61.

[20] Zhu, J., Cai, S., and Suo, Z., 2010, Resonant behavior of a membrane of a dielectric elastomer, *International Journal of Solids and Structures*, **47**, pp. 3254–3262.

[21] Falcão, A.F.O., 2000, The shoreline OWC wave power plant at the Azores, in *Proc. of the Fourth European Wave Energy Conference*, Aalborg, Denmark, 4-6 December.

[22] Falcao, A.F.O., and Rodrigues, R.J.A., 2002, Stochastic modelling of OWC wave power plant performance, *Applied Ocean Research*, **24**(2), pp. 59–71.
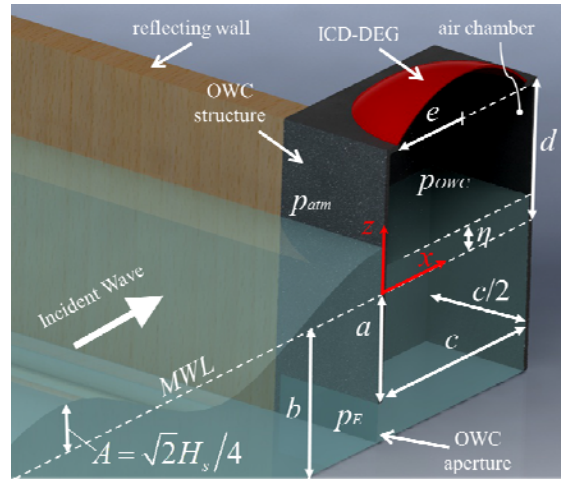
List of Figure Captions:

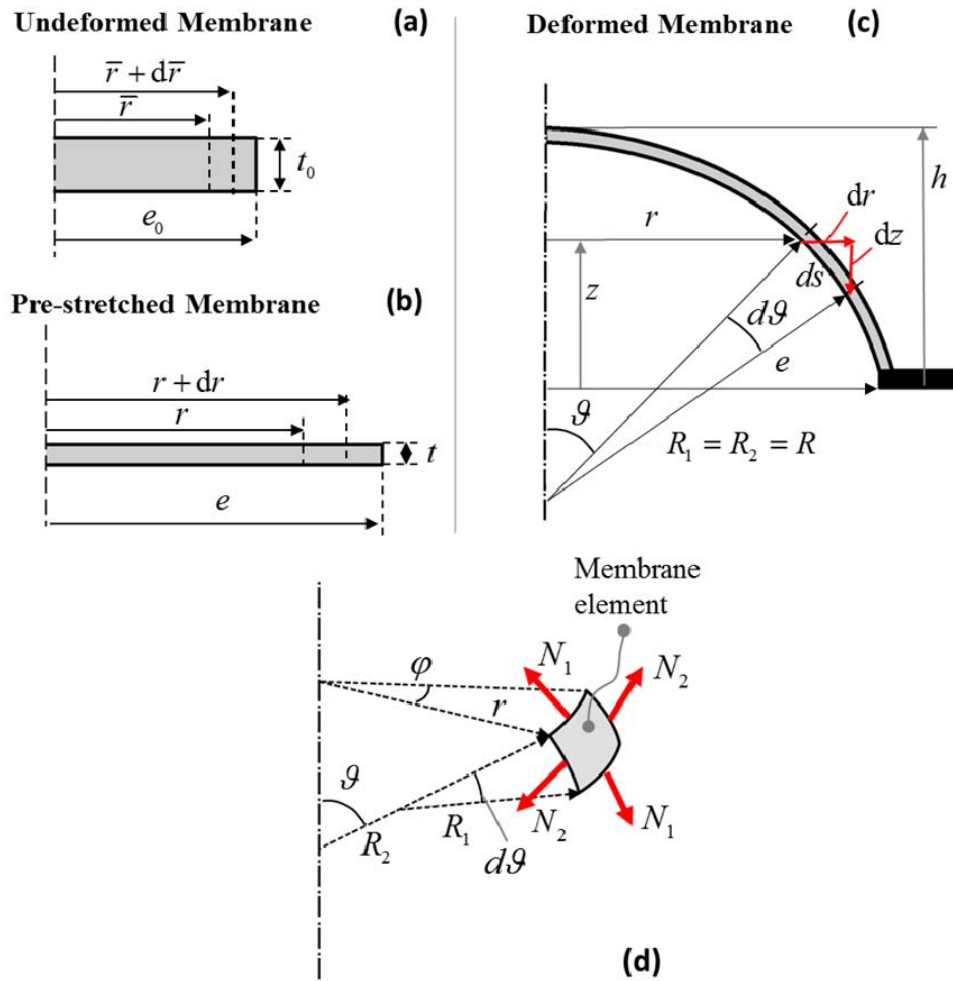Figure 1. Polymeric Oscillating Water Column (Poly-OWC) wave energy converter.

Figure 2. Inflated Circular Diaphragm Dielectric Elastomer Generator (ICD-DEG): a) ICD-DEG undeformed state, b) ICD-DEG pre-stretched state with no differential pressure and electric potential, c) ICD-DEG deformed state with differential pressure and/or electric potential, d) infinitesimal ICD-DEG element.
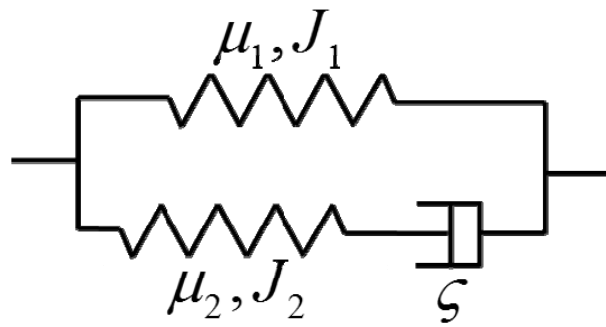
Figure 3. Visco-elastic model for the mechanical response of Dielectric Elastomers: Zener model with two hyper-elastic networks and one dashpot.
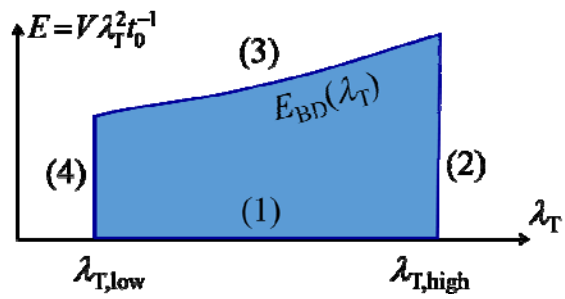
Figure 4: Representation of the considered energy harvesting cycle in the stretch/electric-field plane.

Figure 5: Comparison between FEA and reduced models of the electro-visco-hyperelastic dynamic response of the Inflated Circular Diaphragm Dielectric Elastomer Generator (ICD-DEG): tip displacement h versus time τ.

Figure 6. Energy harvested per cycle by the Poly-OWC with ICD-DEG power take-off as function of ICD-DEG initial tip height h_0 and pre-stretch λ_p. Different plots are for different ICD-DEG thicknesses t (measured at $h = 0$).

Figure 7. Energy harvested per cycle by the Poly-OWC with ICD-DEG power take-off as function of ICD-DEG initial tip height h_0 and pre-stretch λ_p. Different plots are for the same ICD-DEG thickness t (measured at $h = 0$), but for different sea-state conditions.

Figure 1. Polymeric Oscillating Water Column (Poly-OWC) wave energy converter.

Figure 2. Inflated Circular Diaphragm Dielectric Elastomer Generator (ICD-DEG): a) ICD-DEG undeformed state, b) ICD-DEG pre-stretched state with no differential pressure and electric potential, c) ICD-DEG deformed state with differential pressure and/or electric potential, d) infinitesimal ICD-DEG element.

Figure 3. Visco-elastic model for the mechanical response of Dielectric Elastomers: Zener model with two hyper-elastic networks and one dashpot.

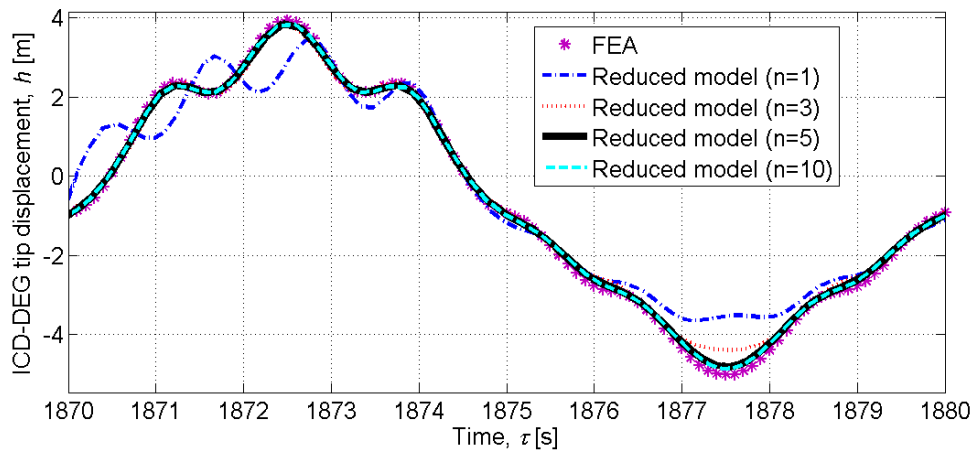Figure 4: Representation of the considered energy harvesting cycle in the stretch/electric-field plane.

Figure 5: Comparison between FEA and reduced models of the electro-visco-hyperelastic dynamic response of the Inflated Circular Diaphragm Dielectric Elastomer Generator (ICD-DEG): tip displacement *h* versus time τ.
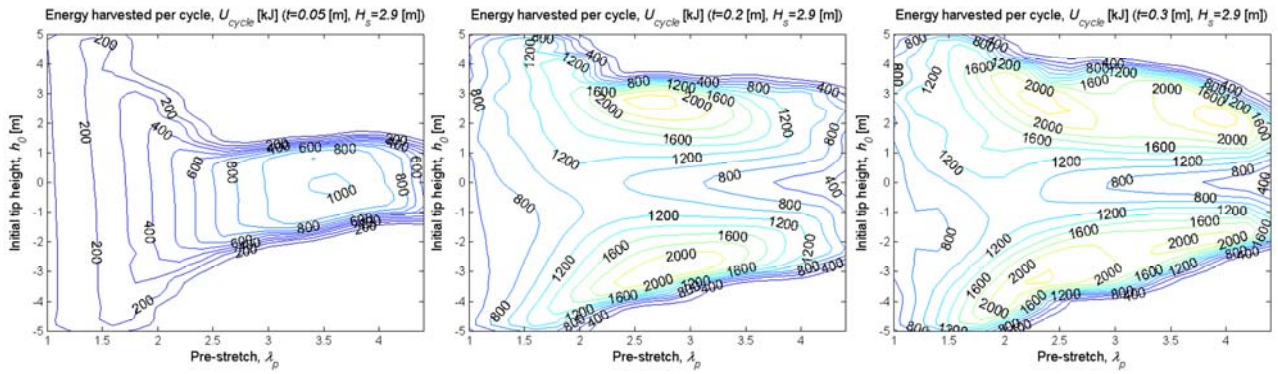
Figure 6. Energy harvested per cycle by the Poly-OWC with ICD-DEG power take-off as function of ICD-DEG initial tip height h_0 and pre-stretch λ_p. Different plots are for different ICD-DEG thicknesses t (measured at $h = 0$).
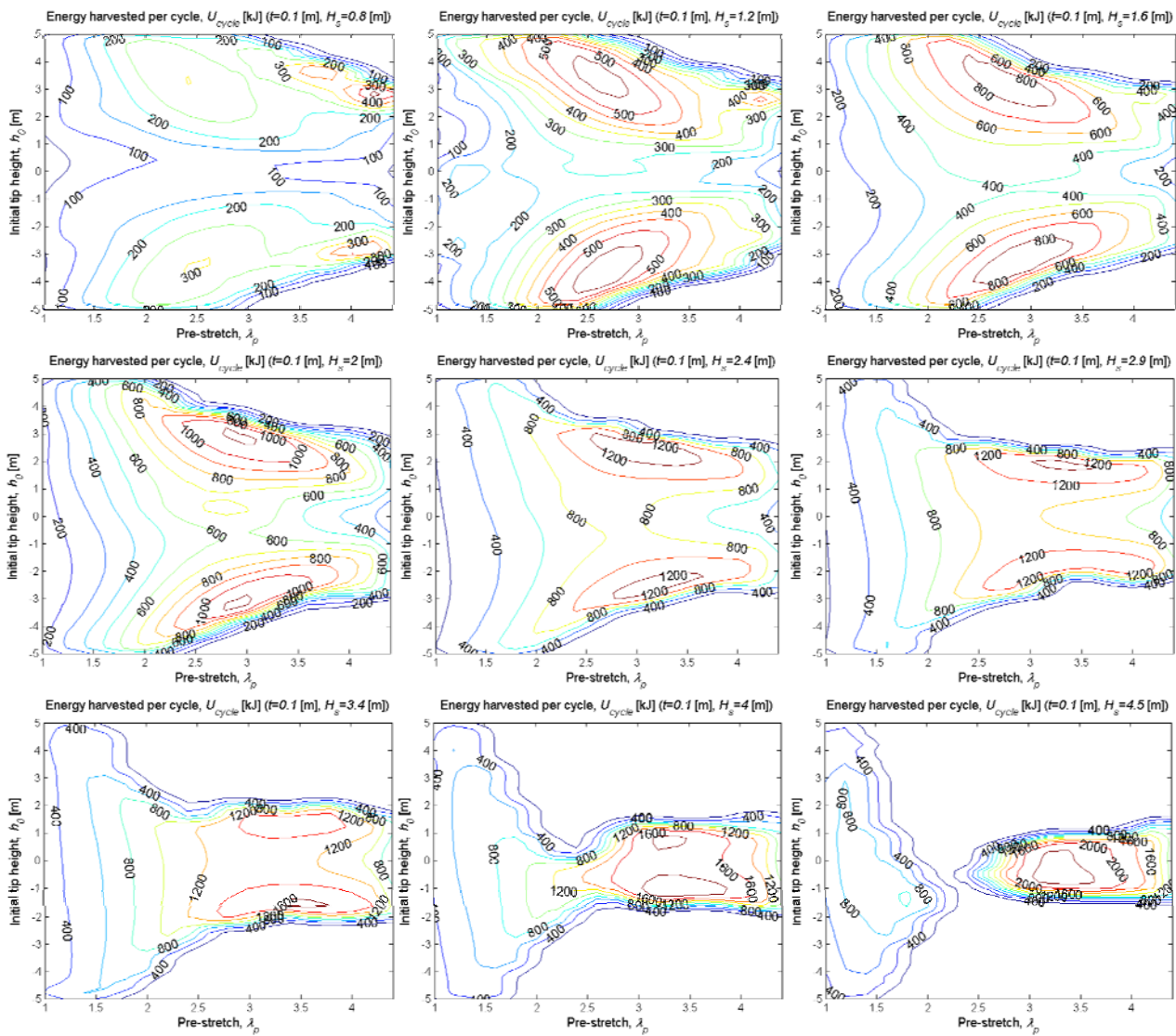
Figure 7. Energy harvested per cycle by the Poly-OWC with ICD-DEG power take-off as function of ICD-DEG initial tip height h_0 and pre-stretch λ_p. Different plots are for the same ICD-DEG thickness t (measured at $h = 0$), but for different sea-state conditions.